CELL BIOLOGY

Spectrin mediates 3D-specific matrix stress-relaxation response in neural stem cell lineage commitment

Eric Qiao[1]†, Jieung Baek[2,3]†, Camille Fulmore[4], Myoung Song[5], Taek-Soo Kim[5], Sanjay Kumar[1,2,6]*, David V. Schaffer[1,2,7]*

While extracellular matrix (ECM) stress relaxation is increasingly appreciated to regulate stem cell fate commitment and other behaviors, much remains unknown about how cells process stress-relaxation cues in tissue-like three-dimensional (3D) geometries versus traditional 2D cell culture. Here, we develop an oligonucleotide-crosslinked hyaluronic acid–based ECM platform with tunable stress relaxation properties capable of use in either 2D or 3D. Strikingly, stress relaxation favors neural stem cell (NSC) neurogenesis in 3D but suppresses it in 2D. RNA sequencing and functional studies implicate the membrane-associated protein spectrin as a key 3D-specific transducer of stress-relaxation cues. Confining stress drives spectrin's recruitment to the F-actin cytoskeleton, where it mechanically reinforces the cortex and potentiates mechanotransductive signaling. Increased spectrin expression is also accompanied by increased expression of the transcription factor EGR1, which we previously showed mediates NSC stiffness-dependent lineage commitment in 3D. Our work highlights spectrin as an important molecular sensor and transducer of 3D stress-relaxation cues.

INTRODUCTION

Mechanical cues from the extracellular matrix (ECM) have emerged as important determinants of stem cell fate commitment. It is now widely accepted that mechanical cues like those arising from substrate elastic properties such as stiffness can influence cell spreading (*1*–*3*), internal cell mechanics (*4*, *5*), and differentiation (*6*–*8*). However, most tissues are viscoelastic rather than elastic, in that they can dissipate as well as store applied stress (*9*, *10*). Substrate stress relaxation is increasingly understood to strongly regulate a number of cell behaviors including mesenchymal stem cell (MSC) spreading (*11*) and differentiation (*12*). Because many traditional culture platforms emphasize tunability of elastic properties (*13*), there has been strong interest in developing a complementary set of materials with tunable viscous or stress-relaxation properties, such as ionically crosslinked hydrogels (*14*) and covalently adaptable networked (CAN) materials (*15*), to achieve tunable viscoelastic properties.

Understanding the influence of ECM viscoelastic properties on phenotype has been complicated by ECM dimensionality. Cells adherent to a two-dimensional (2D) surface experience a different mechanical microenvironment than those fully encapsulated in a 3D biomaterial, even if the bulk mechanical properties of the 2D surface and 3D matrix are similar. Whereas many 2D studies have focused on cell-matrix adhesions as key mediators of stiffness response (*16*–*18*), it has been challenging to extrapolate these mechanisms to 3D. A key distinction of 3D geometries relative to 2D is that cells in 3D compress the surrounding matrix during expansion and growth, giving rise to a confining stress that can trigger mechanotransductive signaling. Matrix stress relaxation might be expected to attenuate this confining stress through dissipation of compressive force, leading to differing effects of stress relaxation in 3D versus 2D.

We recently showed that 3D ECM stiffness responses are mediated by 3D-specific molecular mechanisms that do not require provision of exogenous ECM peptide ligands and involve mobilization of transcription factors that are not appreciably expressed in 2D (*19*). Specifically, increasing the stiffness of purely elastic 3D ECMs suppresses neural stem cell (NSC) neurogenesis through a mechanism driven by the immediate-early transcription factor early growth response protein 1 (EGR1). While EGR1 up-regulation and neurosuppression are accompanied by and depend on the greater confining stress experienced in stiffer 3D matrices, the proximal sensor of confining stress within the cortical cytoskeleton has remained unclear. Additionally, it remains unknown how the introduction of stress-relaxation properties characteristic of tissue would modulate NSC neurosuppression by ECM mechanics.

Here, we investigate the relationship between stress relaxation and mechanosensitive stem cell lineage commitment in 3D matrices, and how these effects present differently in 3D versus 2D. In this regard, we chose to focus on neurogenic versus astrocytic fate, as our previous work had demonstrated that while NSCs can, in principle, generate oligodendrocytes, astrocytes, and neurons, the latter two showed the greatest variation with matrix mechanical properties like stiffness, with oligodendrogenesis levels being low regardless of stiffness (*20*). To investigate how viscoelastic properties affect neurogenesis and astrogenesis, we introduce a hyaluronic acid (HA) hydrogel system in which stress relaxation may be modulated using defined combinations of covalent and noncovalent oligonucleotide-based crosslinks. We then used this system to investigate the role of stress relaxation in alleviating cell confining stress in 3D matrices and compare outcomes with 2D matrices. Stress relaxation enhances rather than suppresses neurogenesis in 3D, whereas stress relaxation reduces neurogenesis on 2D matrices. These 2D-versus-3D differences are accompanied by distinct stress-relaxation effects on actin cytoskeletal assembly and RhoA activation dynamics. RNA

[1]Department of Chemical and Biomolecular Engineering, University of California, Berkeley, Berkeley, CA 94720, USA. [2]Department of Bioengineering, University of California, Berkeley, Berkeley, CA 94720, USA. [3]Department of Mechanical and Biomedical Engineering, Graduate Program in System Health Science and Engineering, Ewha Womans University, Seoul 03760, Republic of Korea. [4]Department of Molecular and Cell Biology, University of California, Berkeley, Berkeley, CA 94720, USA. [5]Department of Mechanical Engineering, Korea Advanced Institute of Science and Technology (KAIST), 291 Daehak-ro, Yuseong-gu, Daejeon 34141, Republic of Korea. [6]Department of Bioengineering and Therapeutic Sciences, University of California, San Francisco, San Francisco, CA 94143, USA. [7]Helen Wills Neuroscience Institute, Berkeley, CA 94720, USA.
*Corresponding author. Email: skumar@berkeley.edu (S.K.); schaffer@berkeley.edu (D.V.S.)
†These authors contributed equally to this work.

sequencing reveals down-regulation of the cortical cytoskeletal protein β spectrin II (spectrin) in 3D matrices with greater stress-relaxing character. When spectrin expression was suppressed, NSC neurogenesis became less sensitive to stress relaxation in 3D, with neurogenesis remaining high even in stiff, non–stress-relaxing 3D matrices. We also observed an increased association between F-actin and spectrin within stress-relaxing environments as well as changes in overall actin polymerization with varying spectrin expression levels. Finally, we found that manipulating spectrin expression led to changes in EGR1 levels, suggesting that spectrin is necessary for robust EGR1 expression, which then drives suppression of neurogenesis in confining matrices.

RESULTS

Mismatched DNA crosslinker sequences relax stress in 3D HA gels

To create a 3D stress-relaxing hydrogel culture system, we chose HA as the scaffold due to its prevalence in brain ECM (*21*) and its wide range of available chemical functionalities (*22*–*24*). Covalent and noncovalent crosslinks were combined to induce stress relaxation. HA functionalized with dibenzocyclooctyne (HA-DBCO) coupled with strain-promoted alkyne-azide cycloaddition (SPAAC) click chemistry was used to attach azide-functionalized crosslinkers and bioactive molecules (Fig. 1A). For crosslinking, we used polyethylene glycol-azide (PEG-az) as a covalent crosslinker and azide-functionalized DNA as noncovalent DNA crosslinkers. DNA crosslinks are composed of two azide-functionalized side arms (SA1-az and SA2-az) crosslinked with a DNA linker, a strategy we have previously reported [(*25*), see note added in proof]. In this system, the DNA linker can be perfectly base pair–matched with the side arms (L0), or it can include a defined number of base-pair mismatches (e.g., L4 for four base-pair mismatches). These mismatches enable the crosslinks to dissociate and reform under applied strains, allowing for stress relaxation while maintaining stiffness. Henceforth, 3D HA-DBCO gels containing DNA will be referred to as 3D/L0 or 3D/L4 depending on the DNA linker used, while 2D gels will be referred to as 2D/L0 or 2D/L4 gels. To facilitate cell-ECM interactions in 3D, we incorporated azide-functionalized arginylglycylaspartic acid peptides (RGD-az) homogeneously throughout the gel. In 3D/L4 gels, we were able to achieve approximately 30% relaxation of initial stress in a bulk rheometry stress-relaxation test (Fig. 1C). Crucially, the stiffness of DNA-crosslinked HA-DBCO gels does not significantly differ from DNA-free gels, regardless of linker sequence (Fig. 1B). In previous studies of 3D mechanosensitive NSC differentiation, we had identified confining stress as a mechanical cue driving stiffness-dependent fate commitment in 3D. To gauge the extent to which bulk stress-relaxation properties may be influencing confining stress experienced by cells, we performed cell volume measurements in 3D/L4 and non–stress-relaxing 3D/L0 gel conditions. As would be expected in a less confining 3D environment, cell volumes were significantly increased in stress-relaxing conditions compared to static gels (Fig. 1, D and E). Cellular sphericity was not significantly altered by ECM stress relaxation, indicating that cells expand isotropically in stress-relaxing matrices (Fig. 1F).

To further characterize the change in confining stress experienced by encapsulated NSCs, we performed finite element analysis to model confining stress over time in 3D/L0 and 3D/L4 gels. Using bulk rheometry data and cell volume measurements, we find that after 24 hours of encapsulation and growth in a stress-relaxing substrate, NSCs experience roughly 60% of the confining stress of NSCs cultured in nonrelaxing substrates (Fig. 1G). These data suggest that hybrid crosslinking can induce stress relaxation in HA gels to an extent that significantly influences the level of confining stress experienced by NSCs in 3D matrices.

NSCs exhibit 3D-specific actin polymerization and fate commitment behaviors in stress-relaxing materials

Under differing confinement conditions, we expect cells to adopt different morphologies and spreading behaviors. In line with this, we saw a significant difference in cellular morphology between 2D and 3D gels, with more protrusions being formed by neurons in the unconfined 2D environment compared to the more rounded shape we observed in 3D matrices (Fig. 2A). Furthermore, we observed that while NSCs exhibited increased cross-sectional areas for stress-relaxing materials in both 2D and 3D, they showed a 3D-specific decrease in F-actin intensity when in stress-relaxing matrices (Fig. 2C). This is consistent with the idea that the assembly of F-actin within the cortical cytoskeleton helps resist confining stress in 3D (*26*, *27*) such that the most intense F-actin polymerization should occur in the most confining conditions. Together, these results reinforce the notion that distinct mechanosensing mechanisms are driving cell responses in 2D and 3D matrices.

Next, we compared the differentiation behavior of NSCs on 2D HA-DBCO gels and in 3D HA-DBCO gels. As in previous differentiation studies, NSCs were cultured in mixed differentiation medium conditions for 7 days before staining for a neuronal (β-tubulin III) or astrocyte marker [glial fibrillary acidic protein (GFAP)]. We observed a striking difference in fate commitment in 3D gels, with a significant increase in neurogenesis from ~40% β-tubulin III$^+$ in 3D/L0 compared to ~55% β-tubulin III$^+$ in 3D/L4 gels. We also noted a corresponding decrease in astrogenesis from ~45% GFAP$^+$ in 3D/L0 compared to ~30% GFAP$^+$ in 3D/L4 gels. This contrasts starkly with NSCs differentiated on 2D stress-relaxing substrates, where neurogenesis was reduced and astrogenesis increased (Fig. 2B). Additionally, when NSCs were exposed to a hyperosmotic PEG-containing medium during the first 48 hours of differentiation, cell volume fell in all gel conditions relative to L4 conditions, and there was no increase in neurogenesis or reduction in astrogenesis in stress-relaxing gels. These results strongly indicate that relaxation of volume restriction in stress-relaxing gels plays a critical role in the observed phenotype (fig. S3). Together, these data indicate that the subsequent enhancement of neurogenesis in 3D stress-relaxing gels relative to both 2D stress-relaxing gels and 3D nonrelaxing gels is due to a dimensionality-dependent volume-confinement effect, and not differences in HA engagement to cell surface receptors.

Spectrin is up-regulated in gels with higher confining stress

We hypothesized that the observed opposite trends in stress relaxation–dependent lineage commitment in 2D versus 3D matrices may be primarily due to a 3D matrix-specific confining stress, particularly since confining stress is present only in 3D conditions, and ABAQUS simulations indicated that stress relaxation leads to a significant decrease in experienced confining stress after just 24 hours of encapsulation (Fig. 1G). Furthermore, we theorized that the cortical actin cytoskeleton may be more directly recruited in 3D than in 2D given the importance of confining stress in 3D and thus play a more prominent role in transducing mechanical signals to regulate fate decisions.

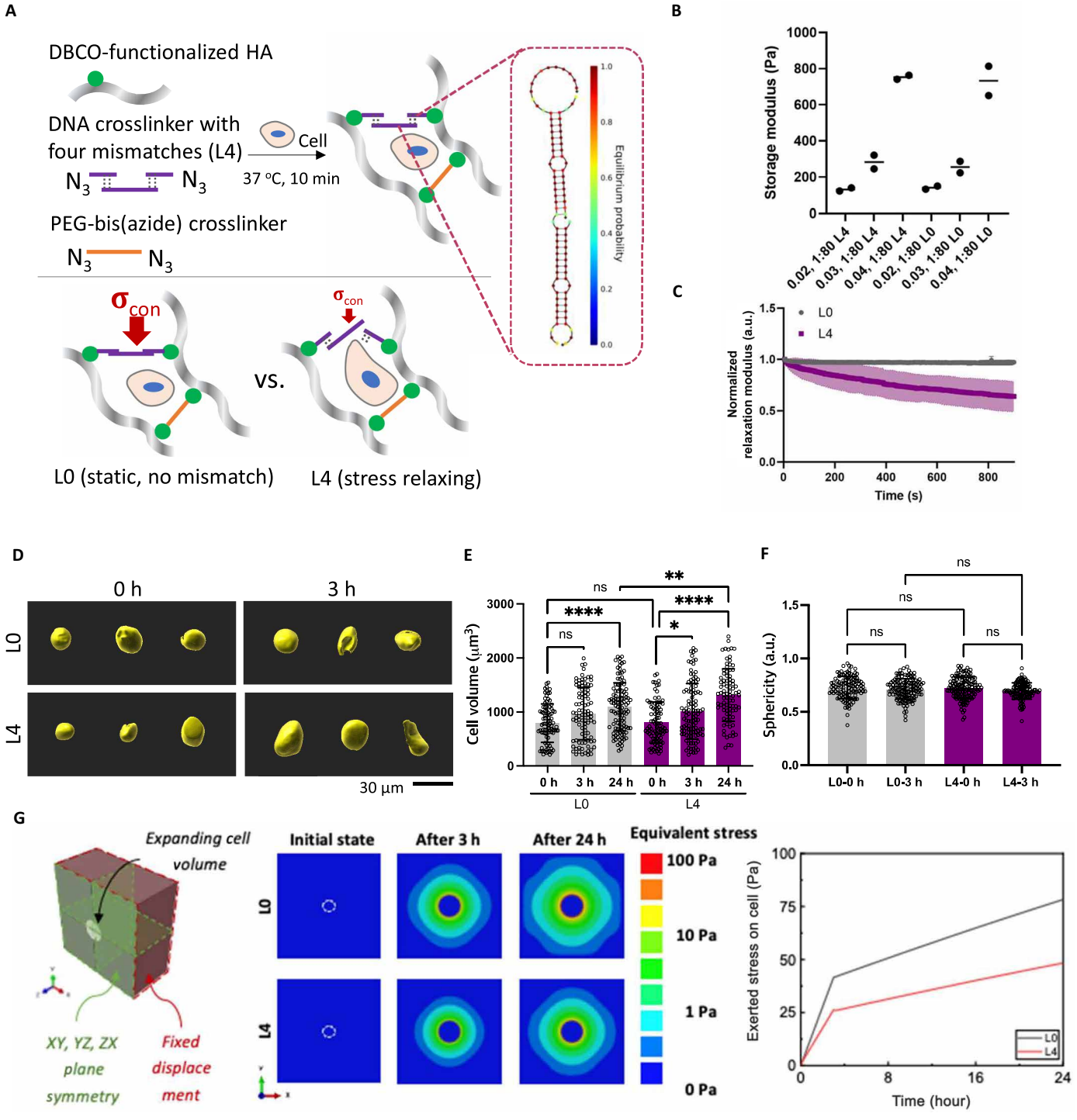

Fig. 1. Mismatched DNA crosslinkers relax stress in 3D HA gels. (**A**) Schematics of dual crosslinked HA gels. Gels contain PEG-based covalent and DNA-based noncovalent crosslinks. L4 gels contain DNA crosslinks with base-pair mismatches to allow release of confining stress, while L0 gels contain perfectly base pair–matched DNA crosslinks. (**B**) Shear storage modulus of dual crosslinked L0 and L4 gels using a covalent:noncovalent crosslink ratio of 1:80 and varying ratios of covalent:HA monomer (0.02, 0.03, 0.04). (**C**) Relaxation modulus over time of 1:80 L0 and L4 gels under constant shear strain (15%). (**D**) Visualization of cell volumes in L0 and L4 gels. NSCs stained with membrane dye and cell volumes measured 3 and 24 hours after encapsulation. Scale bar, 30 µm. Quantification of cell volumes (**E**) and cell sphericity (**F**) in L0 and L4 gels. $n = 86$ to 111 single cells. One-way ANOVA with Tukey post hoc test. $^{****}P < 0.001$, $^{***}P < 0.005$, $^{**}P < 0.01$, $^{*}P < 0.05$. (**G**) ABAQUS simulation to model matrix confining stress during cell volumetric growth in L0 and L4 gels.

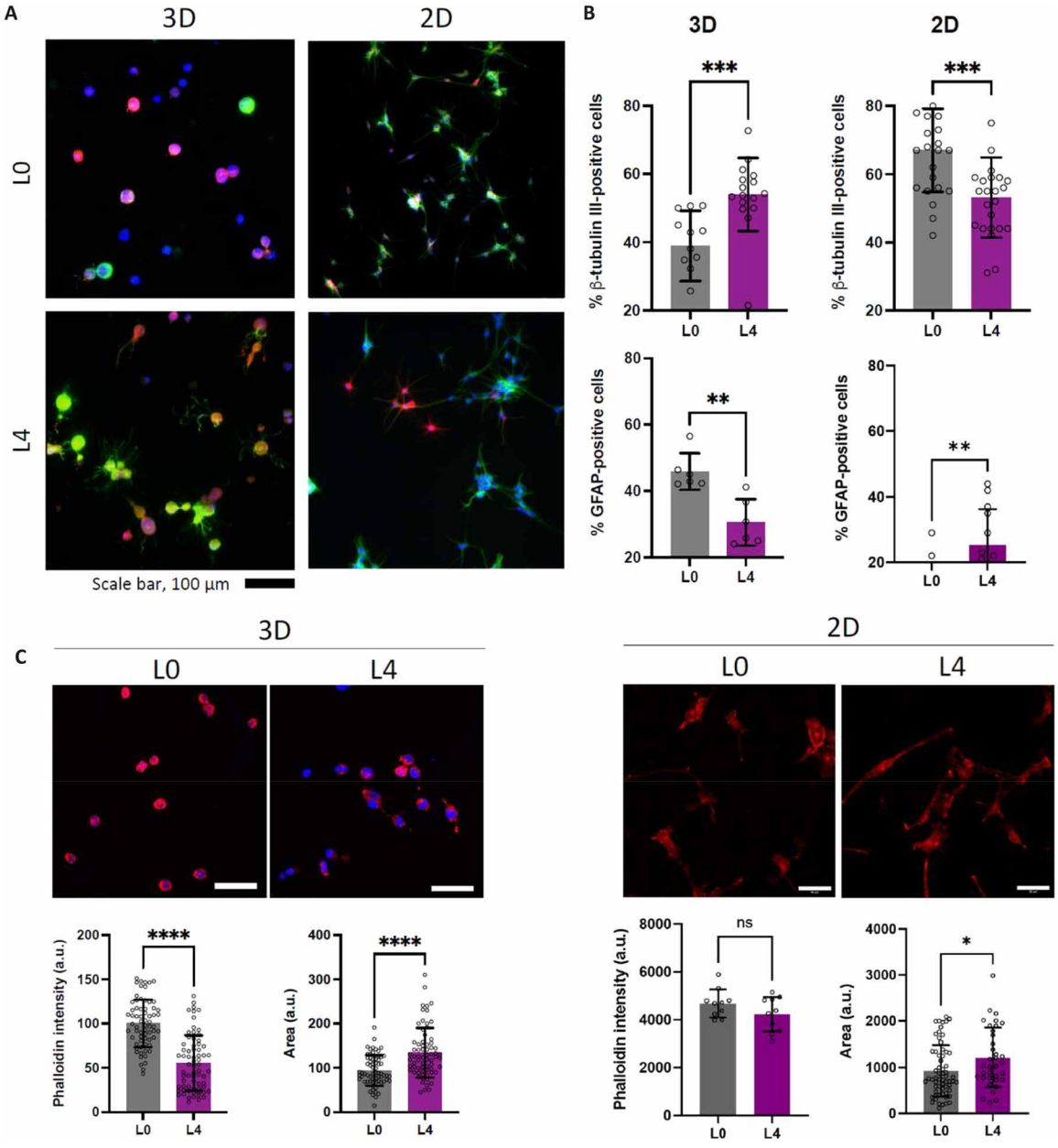

Fig. 2. NSCs cultured in 3D and 2D HA gels exhibit opposite trends in neurogenesis and mechanotransduction under the stress relaxation. (**A**) Representative images of immunostaining of NSCs for β-tubulin III (green), GFAP (red), and DAPI (blue) in L0/3D, L4/3D, L0/2D, and L4/2D gels. Scale bar, 100 μm. (**B**) Quantification of β-tubulin III–positive and GFAP-positive cells in L0/3D, L4/3D, L0/2D, and L4/2D gels. $n = 6$ to 24 biological replicates. (**C**) Representative images of staining for F-actin (red) and DAPI (blue). Scale bar, 100 μm. Quantification of integrated F-actin intensity normalized by cell area in L0/3D, L4/3D, L0/2D, and L4/2D gels. $n = 15$ to 66 single cells. a.u., arbitrary units.

Specifically, we found from previously published RNA-sequencing (RNA-seq) analyses that expression of a set of genes involved in membrane cytoskeletal formation was highly up-regulated in 3D stiff gels (1200 Pa) with high confining stress than in 3D soft gels (100 Pa) with low confining stress (*19*). However, these previous data operate using stiffness as a proxy for confining stress, which, while reasonable, does not isolate base stiffness from confining stress like a stress-relaxing system does.

We proceeded to investigate whether *Sptbn1* (spectrin β, non-erythrocytic 1), one of the top differentially expressed genes in stiff versus soft 3D matrices, contributed to the divergent stress-relaxation responses in between 2D and 3D matrices. *Sptbn1* encodes the protein β spectrin II (SPTBN1), the most common isoform of non-erythrocyte spectrin that functions in actin crosslinking and linking of the plasma membrane to the actin cytoskeleton (*28*, *29*).

To assess whether protein expression levels of β spectrin II varied based on differences in confining stress independent of stiffness effects per se, we measured β spectrin II levels by Western blot in four hydrogel conditions (2D/L0, 2D/L4, 3D/L0, and 3D/L4). Consistent with transcript-level expression from RNA-seq in which we observed

higher *Sptbn1* expression in confining matrices (stiff, 1200 Pa) (*19*), we observed higher β spectrin II protein levels in nonrelaxing 3D gels (3D/L0) than in stress-relaxing gels (3D/L4) (Fig. 3B). Overall expression levels of β spectrin II in both 2D gel conditions (2D/L0 and 2D/L4) were lower compared to levels in 3D/L0 gels. To evaluate whether stress relaxation affected not only the expression but also the localization of β spectrin II, we immunostained for β spectrin II (Fig. 3C). Consistent with Western blotting (Fig. 3, A and B), the fluorescence intensity of β spectrin II was higher in the cells within 3D static gels (3D/L0) than in those within 2D gels (2D/L0 and 2D/L4). Furthermore, profiling of the fluorescence intensity revealed strikingly different distributions of β spectrin II in cells as a function of dimensionality and stiffness (Fig. 3D). β Spectrin II expression in 3D gels showed preferential, condensed localization to the cell boundary, whereas cells in 2D did not show a stiffness-dependent bias in distribution Together, the much lower expression of β spectrin II in 2D versus 3D (irrespective of stiffness) suggests that spectrin's role is 3D specific. Furthermore, the reduction in spectrin expression in stress-relaxing 3D/L4 gels implies that mechanical confining stress regulates spectrin activity in 3D.

Spectrin regulates stress relaxation–dependent neurogenesis only in 3D

To investigate the potential role of β spectrin II in stress relaxation–dependent NSC fate commitment in 3D gels, we depleted *Sptbn1* gene expression with lentiviral short hairpin RNAs (shRNAs) (Fig. 3E). Two shRNAs (shSptbn1-1 and shSptbn1-2) targeting different regions of *Sptbn1* mRNA transcript efficiently knocked down β spectrin II protein expression compared to cells transduced with a control shRNA with a scrambled sequence (shCtrl). We then repeated differentiation assays with these cells in four different gels: 2D/L0, 2D/L4, 3D/L0, and 3D/L4. No significant difference in neurogenesis among naïve, shCtrl, and shSptbn1-1 cells was detected in 2D (Fig. 3F). This is consistent with the negligible stress relaxation–independent β spectrin II expression seen previously on 2D gels. In contrast, *Sptbn1* knockdown (shSptbn1-1 and shSptbn1-2) rescued the lower neurogenesis in cells in 3D/L0 gels compared with shCtrl and naïve cells to levels similar to values seen on stress-relaxing gels (3D/L4) (Fig. 3, G and H). We also note a reduction in overall cell volume and sphericity in encapsulated spectrin knockdown NSCs, in line with the previously established role of spectrin in mechanically stabilizing cell morphology (fig. S4). This further supports the notion that *Sptbn1* mediates stress relaxation–dependent NSC fate choice only in 3D gels and not 2D gels.

Spectrin recruits cortical actin cytoskeleton in a confined microenvironment

We next explored how *Sptbn1* expression influences cell mechanosensitivity and thereby regulates NSC lineage commitment in 3D. β Spectrin II contains multiple actin-binding domains (ABDs), which allow β spectrin to interact with F-actin in a number of settings, including through the membrane-associated actin-spectrin cytoskeleton, which is known to regulate the morphology of dendrites and other neuronal processes (*30*, *31*). Furthermore, we have previously found that cytoskeleton-binding proteins such as angiomotin play an important role in mechanosensitive NSC lineage commitment (*32*). On the basis of these data, we hypothesized that differences in actin cytoskeletal formation in 3D/L0 gels compared to 3D/L4 gels may be due to stress relaxation–dependent *Sptbn1* expression patterns, which in turn influence fate commitment. To assess the importance of *Sptbn1* in actin cytoskeleton formation, F-actin was stained by phalloidin, and its fluorescence intensity was quantified in shCtrl and shSptbn1-1 cells encapsulated in four different gels: 2D/L0. 2D/L4, 3D/L0, and 3D/L4 (Fig. 4, A to D). Sptbn1 knockdown strikingly affected cytoskeletal formation in 2D and 3D conditions. In 2D, we observed a significant decrease in F-actin staining intensity in stress-relaxing L4 gels with *Sptbn1* knockdown. In contrast, in 3D conditions, we saw a significant decrease in F-actin staining in static L0 gels with *Sptbn1* knockdown, while the change in F-actin intensity was negligible in L4 gels. These results demonstrate that spectrin contributes to opposing trends of actin polymerization in a manner that is stress relaxation and dimensionality dependent. Although *Sptbn1* knockdown did not significantly change cell fate in 2D gels, it is likely that *Sptbn1* knockdown allows for higher neurogenesis in nonrelaxing conditions in 3D.

In addition, we performed structured illumination microscopy (SIM) to assess whether the degree of interaction between actin and β spectrin II in nonrelaxing and stress-relaxing 3D gel conditions changed upon *Sptbn1* knockdown (Fig. 4E and movies S1 and S2). We measured the degree of colocalization of actin and β spectrin II using a Mander's overlap coefficient ($M_{sp/ac}$), which is proportional to the degree of β spectrin II signal overlapping with actin signal across the whole cell (Fig. 4F). A significant degree of colocalization of actin and β spectrin II was seen in confining 3D environments, and a significant decrease in the degree of colocalization was observed under stress-relaxing conditions. In β spectrin II knockdown cells, the residual β spectrin II did not exhibit altered levels of colocalization between relaxing and nonrelaxing conditions, although the low levels of β spectrin II expression rendered this analysis less unreliable.

β spectrin II and EGR1 positively influence one another's expression in regulating neurogenesis in 3D

Having established differential expression patterns of β spectrin II and a role in both influencing fate commitment and cytoskeletal formation in relaxing and nonrelaxing matrices, we investigated what potential downstream interactions β spectrin II may have with other mechanosensitive effectors, in particular EGR1. We previously implicated the *Egr1* gene, which encodes EGR1 protein, as a 3D matrix-specific mediator of mechanosensitive NSC lineage commitment (*19*). We previously showed that EGR1, like β spectrin II here, exhibits low expression in 2D, as well as stiffness and confining stress-dependent expression in 3D and subsequent regulation of the β-catenin signaling pathway (*19*). Furthermore, the expression of EGR1 was highly associated with actin polymerization in 3D matrices. Given that β spectrin II function in 3D matrices also seems to be closely associated with these two phenomena, we examined the relationship between the expression levels of β spectrin II and EGR1.

We carried out coimmunostaining of EGR1 and β spectrin II for EGR-overexpressing cells (pMXs-EGR1) and control cells (pMXs-GFP) in four different gels (2D/L0, 2D/L4, 3D/L0, and 3D/L4) (Fig. 5A). We also quantified the staining intensity of both proteins in encapsulated NSCs to assess the distribution of single cells based on their EGR1 and β spectrin II expression levels (Fig. 5B). As expected, in all the four gel conditions, EGR1 overexpression (pMXs-EGR1) cell populations exhibited higher EGR1 fluorescence intensity than controls (pMXs-GFP), confirming overexpression. We also noted that the overall expression levels of EGR1 in both 2D

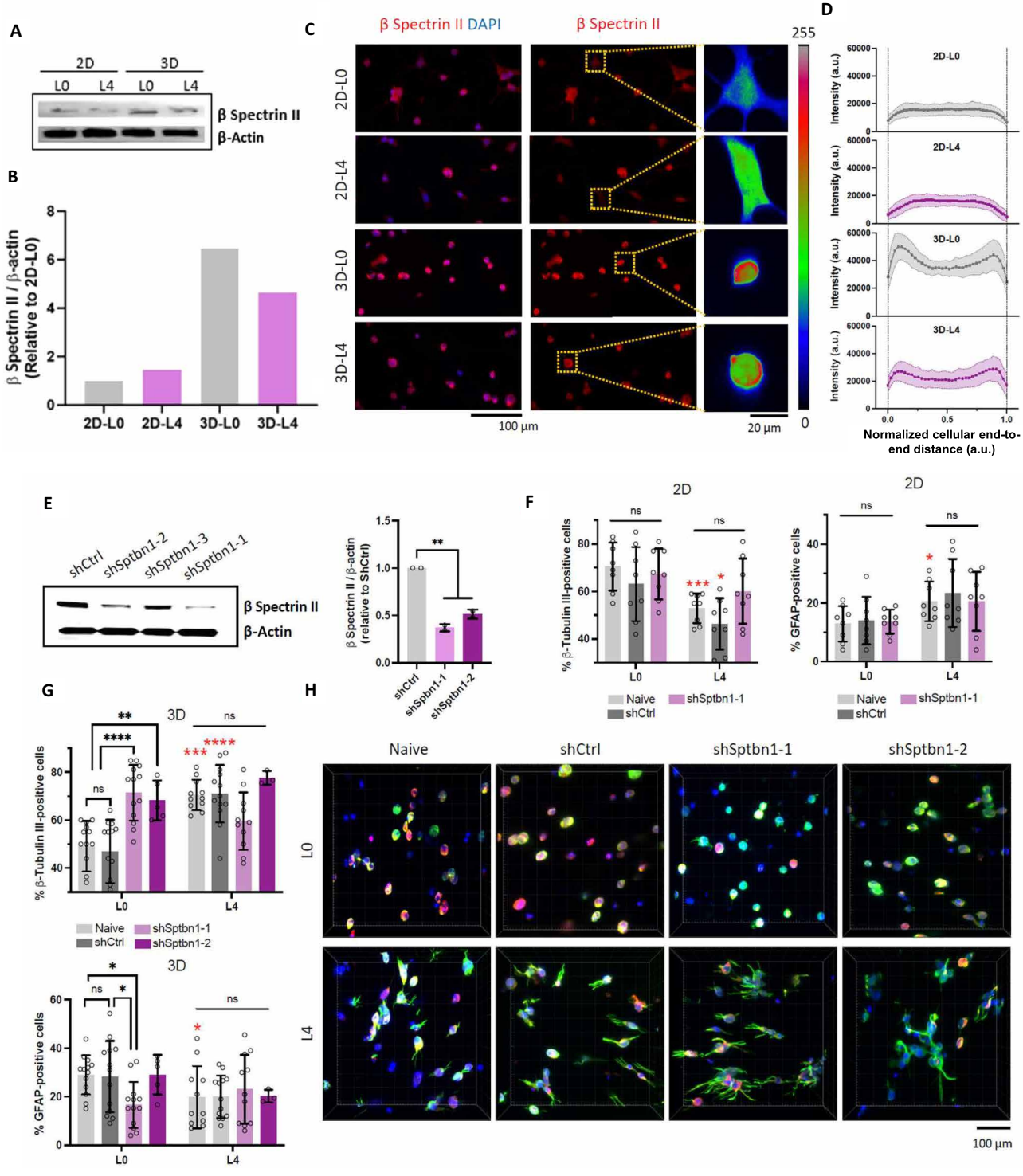

Fig. 3. Spectrin regulates stress relaxation–dependent neurogenesis only in 3D. (**A**) Western blot of β spectrin II protein expression in NSCs incubated in four different gels (2D/L0, 2D/L4, 3D/L0, and 3D/L4) for 24 hours. (**B**) Quantification of Western blot data for spectrin knockdown (KD) cell lines relative to 2D-L0 conditions (**C**) Confocal imaging and (**D**) normalized cellular end-to-end distance-based fluorescence intensity plotting of β spectrin II in the NSCs differentiated in the four different gels. $n < 21$ cells. (**E**) β spectrin II expression after shRNA KD verified by Western blot and the quantification of the band intensities. $n = 2$. Quantification of β-tubulin III–positive and GFAP-positive control (naïve or shCtrl) cells and KD (shSptbn1-1 or shSptbn1-2) cells in 2D/L0 and 2D/L4 (**F**) and 3D/L0 and 3D/L4 (**G**) gels. Red asterisks are from statistical tests based on the comparison between L4 versus L0 for each corresponding cell line. $n = 2$ or 3 biological replicates. (**H**) Representative images of immunostaining for the β-tubulin III (green), GFAP (red), and DAPI (blue) in the four different gels. Scale bar, 100 μm. One-way ANOVA with Tukey post hoc test. ****$P < 0.001$, ***$P < 0.005$, **$P < 0.01$, *$P < 0.05$.

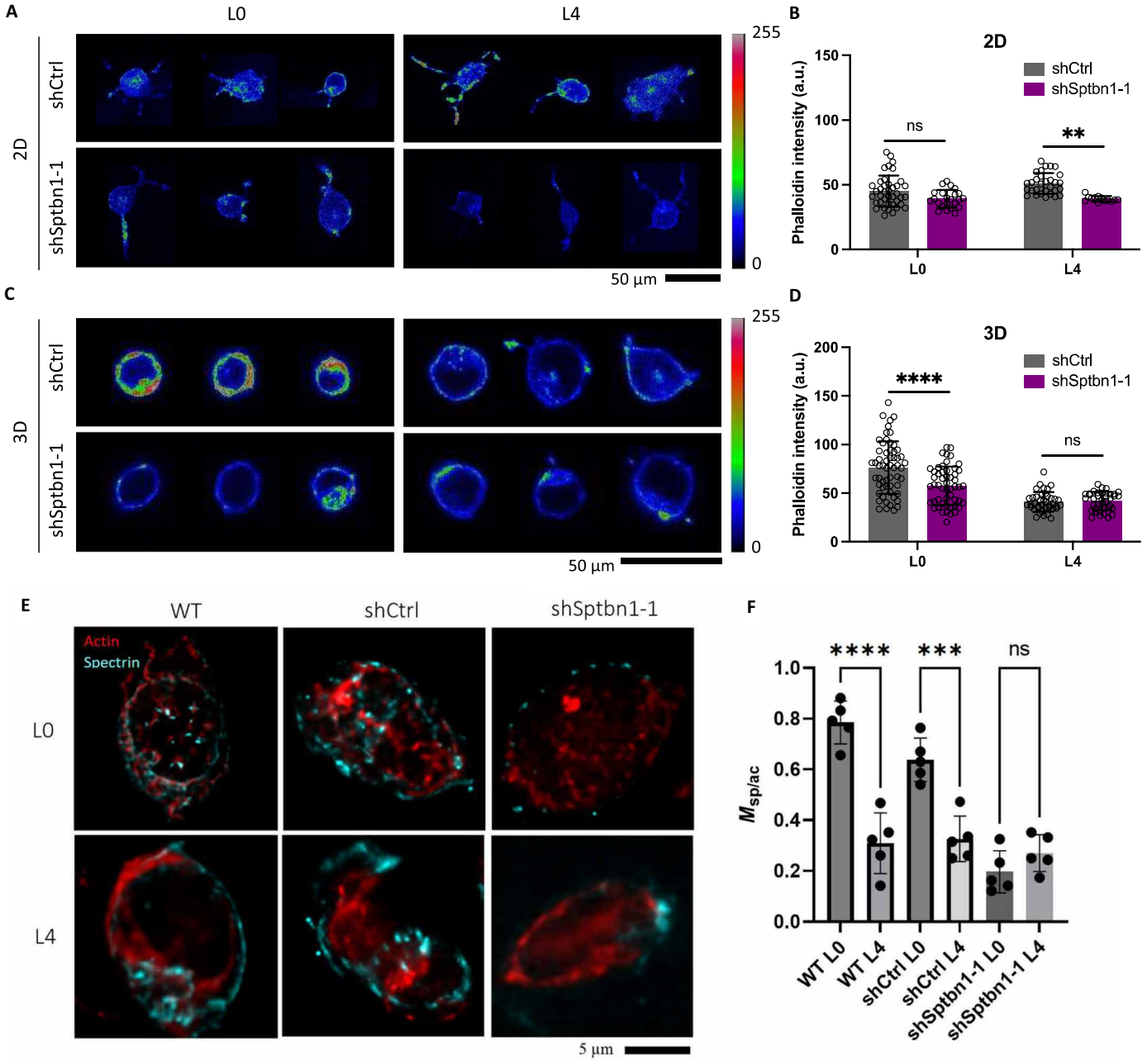

Fig. 4. Spectrin recruits cortical actin cytoskeleton in a confined microenvironment. (**A**) Color-coded representation of phalloidin-stained single shCtrl and shSptbn1-1 (KD) cells in 2D L0 and L4 gels. Scale bar, 100 μm. (**B**) Quantification of phalloidin intensity after background subtraction. (**C**) Color-coded representation of phalloidin-stained single shCtrl and shSptbn1-1 (KD) cells in 3D L0 and L4 gels. Images for 3D gels were obtained after sectioning. Scale bar, 50 μm. (**D**) Quantification of phalloidin intensity after background subtraction. $n > 65$ cells per each 3D condition. (**E**) Representative super-resolution images of NSCs stained for actin and spectrin. Images have been computationally deconvolved. (**F**) Mander's colocalization coefficients for actin/spectrin colocalization. One-way ANOVA with Tukey post hoc test. ****$P < 0.001$, ***$P < 0.005$, **$P < 0.01$, *$P < 0.05$.

gels (2D/L0 and 2D/L4) were strikingly lower than those in 3D gels (3D/L0 and 3D/L4), consistent with our previous findings yet suggesting a posttranscriptional down-regulation mechanism (*19*). This trend was also present in β spectrin II expression levels. Notably, β spectrin II expression levels correlated with EGR1 expression, i.e., EGR1-overexpressed cells (pMXs-EGR1) showed higher expression of β spectrin II in all gel conditions. Conversely, we also investigated if Sptbn1 knockdown influenced EGR1 expression in shCtrl and shSptbn1-1 cells within the four gels. First, we confirmed our Western blotting results (Fig. 3E) in knockdown cells by observing via quantitative polymerase chain reaction (qPCR) that Sptbn1 mRNA levels were significantly lower in shSptn1–1 cells than in shCtrl cells in all the four gel conditions. More interestingly, knockdown of *Sptbn1* significantly decreased EGR1 expression level in both 3D/L0 and

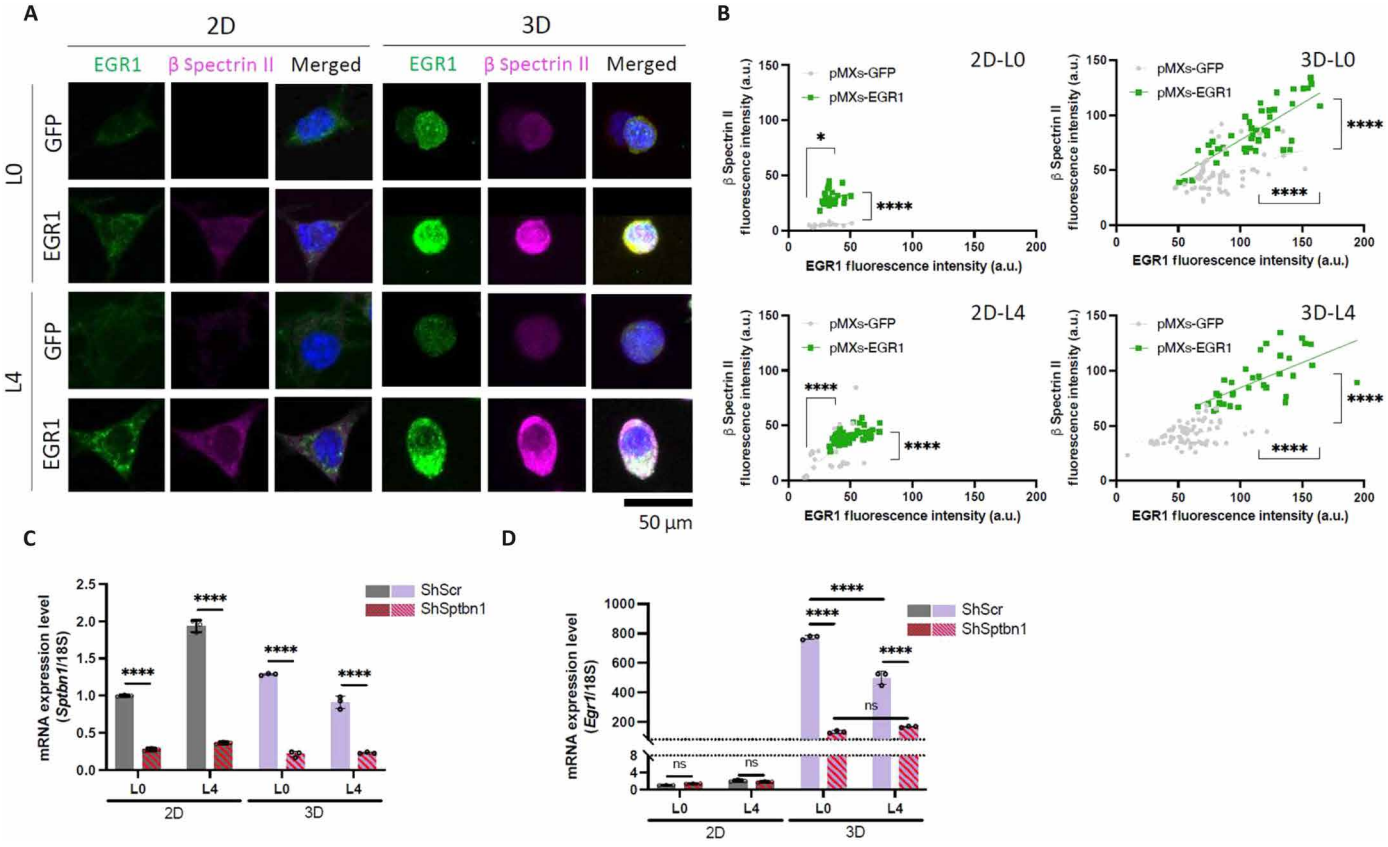

Fig. 5. Spectrin and EGR1 positively affect each other. (**A**) Representative images of immunostaining for EGR1 (green) or β spectrin II (magenta) in control (GFP) and EGR1 overexpression (EGR1) cells under four different gel conditions: 2D/L0, 2D/L4, 3D/L0, and 3D/L4. Scale bar, 50 μm. (**B**) Scatterplot of fluorescence intensity of EGR1 versus β spectrin II in single control (pMXs-GFP) and EGR1 overexpression (pMXs-EGR1) cells in the four gels. $n > 16$ cells and $n > 34$ cells were used for 2D and 3D gels, respectively. mRNA expression level of *Sptbn1* (**C**) and *Egr1* (**D**) in control (shScr) and *Sptbn1* KD (ShSptbn1) cells differentiated in 2D/L0, 2D/L4, 3D/L0, and 3D/L4 gels for 5 hours.

3D/L4 gels, reducing the higher EGR1 expression in 3D/L0 down to a level similar to 3D/L4 gels. Again, this change was present only in 3D gels and not in 2D gels. Together, these results indicate that β spectrin II expression and EGR1 expression positively affected one another across all conditions, but with much more pronounced effects in 3D gels than in 2D gels. Since EGR1 has been shown to restrict neurogenesis in 3D matrices, spectrin may be operating together with EGR1 to drive astrogenesis (Fig. 6).

DISCUSSION

We have investigated the role that substrate stress relaxation plays in mechanosensitive NSC fate commitment in 3D. We did so by using dually crosslinked HA-DBCO hydrogels to generate relaxing and nonrelaxing 3D matrices and observed that, similarly to 2D conditions, stress relaxation exerted a strong effect on NSC fate commitment and cytoskeletal properties, but with the opposite trends from 2D substrates of the same composition. Furthermore, we have established the structural actin-associated protein β spectrin II as a key mediator of confining stress mechanosensing and stress relaxation–dependent fate commitment. We had previously demonstrated that stiffness, rather than adhesive ligand presentation, was the determining factor in stiffness-dependent 3D fate commitment as well as broader transcriptomic changes (*19*). Furthermore, in addition to EGR1, our study also identified β spectrin II as a highly stiffness-dependent protein and a likely regulator of 3D mechanical signals. This study confirms the key role both EGR1 and β spectrin II play in regulating fate commitment in confined environments by demonstrating a direct influence of spectrin on neurogenesis and providing a more complete picture of how confinement signals are transduced.

While there have been previous studies of the impact of stress relaxation on stem cell differentiation in 3D (*33*), a primary mechanism often offered to explain changes in differentiation behavior is integrin-based signaling arising from mechanical remodeling of the matrix by cells (*34*). Here, we offer a different perspective by identifying confining stress as a likely instructive cue toward NSC differentiation. In previous studies of the impacts of confinement on stem cell differentiation, robust changes in cell behavior were observed and linked to integrin signaling (*35*), epigenetic reprogramming (*36*), and dilution of signaling molecules like RhoA (*37*). While our results do not preclude these mechanisms, this study introduces β spectrin II as a key regulator of 3D mechanosensitive fate commitment. Furthermore, our data suggest that volume confinement in 3D through PEG treatment produces similar changes in fate commitment to physical confinement, demonstrating that β spectrin II's role in regulating cell volume plays a role in regulating fate commitment (figs. S3 and S4).

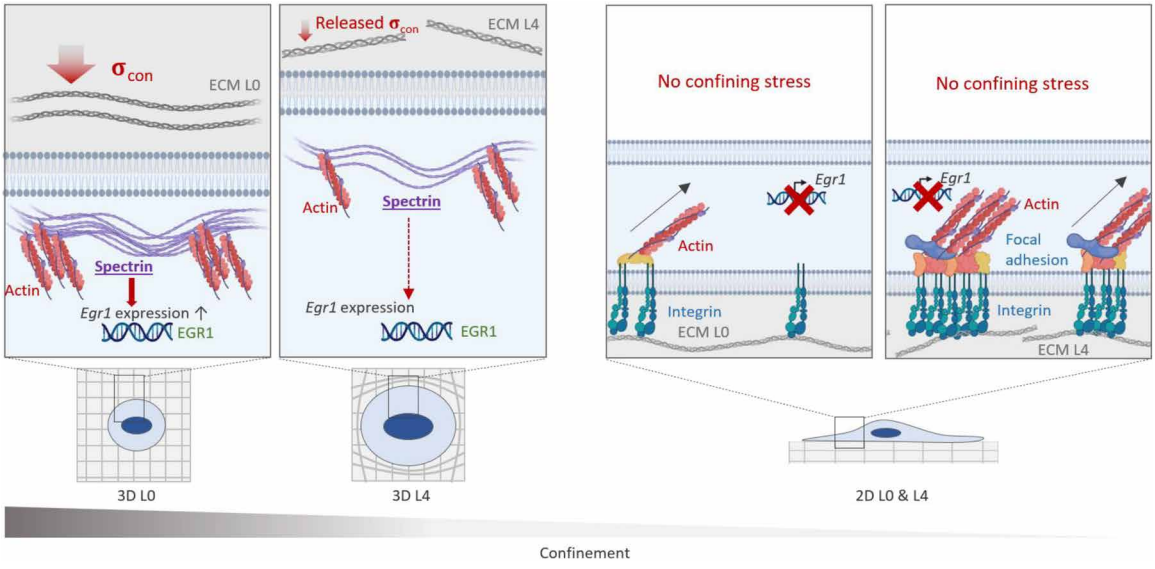

Fig. 6. Relaxation of confinement stress in 3D regulates spectrin-mediated regulation of EGR1. 3D environments, where confining stress, σ, cannot be relaxed over time, lead to up-regulation of spectrin and EGR1 expression. 2D microenvironments do not have appreciable confining stress, and while stress relaxation induces increases in focal adhesion formation and cell area, both spectrin and EGR1 expression remains low. Created with BioRender.com.

We observed that not only does the expression level of β spectrin II vary with both dimensionality and level of confining stress (in 3D) but also the localization of spectrin within the cell changes. We observed a much stronger cortical localization of β spectrin II in 3D nonrelaxing gel conditions compared to 3D stress-relaxing conditions. By contrast, 2D conditions show an overall weaker and more diffuse expression pattern compared to 3D gels. This result is consistent with the idea that β spectrin II's role is tied to confining stress, which would be largely absent in a 2D monolayer culture. Given β spectrin II's known role as part of the membrane-associated periodic cytoskeleton, it is reasonable to suggest that β spectrin II's role in confining environments is to support membrane rigidity and trigger confining stress-activated signaling pathways.

Given the close association between β spectrin II and F-actin, it was also interesting that expression levels of β spectrin II affected expression levels of EGR1, another mechanosensitive protein known to be influenced by actin dynamics, in a 3D-specific manner. While our results indicate a correlation between β spectrin II and EGR1 expression, it is important to note that further studies are required to establish a definitive causal relationship between the expression levels of each. Nonetheless, these results provide an avenue for further study by demonstrating that the expression level of β spectrin II, which is itself dependent on dimensionality and confining stress, influences the expression level of the mechanosensitive differentiation protein EGR1.

Furthermore, the link between β spectrin II and EGR1 presents a possible mechanism for spectrin-mediated fate commitment. Although EGR1 is linked to 3D mechanosensitive differentiation through its downstream impact on β-catenin activity, the direct link between ECM mechanical properties and EGR1 activity was unclear (*19*) as EGR1 is not a known membrane cytoskeleton-associated protein. β Spectrin II may provide a link as a cytoskeletal adaptor protein that is canonically localized to the membranes of cells. Such a role linking cortical cytoskeletal proteins to downstream signaling has been previously identified in other nonerythroid cell types (*38*). Another possibility is that a link exists between EGR1, β spectrin II, and the mechanosensitive Rho GTPase (guanosine triphosphatase) RhoA. Using the previously described RhoA fluorescence resonance energy transfer (FRET) biosensors (*39*), we find that RhoA exhibits oscillations in nonrelaxing matrices (fig. S1, A and B). We had previously observed this phenomenon across 2D gel conditions, both relaxing and nonrelaxing. However, in 3D/L4 gels, we see a marked decrease in the relative amplitude of RhoA oscillations. Given RhoA's previously established role in determining cell fate (*20*), RhoA may also be an important transducer of stress relaxation cues in 3D. This is further supported by the fact that we observe increased astrogenesis in 3D/L0 and 3D/L4 gels when RhoA activation is artificially driven with a period of 600 s (fig. S1, C and D). However, this mechanism still requires further study to confirm.

We propose a mechanism by which increased β spectrin II expression and localization to the membrane in confining environments (such as 3D stiff or nonrelaxing substrates) drives increased EGR1 activity, which in turn suppresses neurogenesis.

MATERIALS AND METHODS

Cell culture and differentiation

Adult rat hippocampal NSCs were isolated previously from adult female Fischer 344 rats (Charles River) as described (*40*) and were cultured in Dulbecco's Modified Eagle Medium (DMEM)/F-12 supplemented with N2 (Thermo Fisher Scientific). Cells were maintained with fibroblast growth factor–2 (FGF-2) (20 ng/ml) (PeproTech) on laminin-coated cell culture plates. A mixed differentiation medium condition with no FGF-2 and 1% fetal bovine serum (FBS) (Corning) + 1 μM retinoic acid (Sigma-Aldrich) was used for differentiation assays. All animal studies are conducted in accordance with National Institutes of Health (NIH) guidelines on animal use and with approval of the UC Berkeley Animal Care and Use Committee.

DBCO functionalization to HA

HA backbones were functionalized with dibenzocyclooctyne (DBCO) groups as previously described (*41*). Briefly, 500 mg of 60-kDa HA (Lifecore) was reacted with 143 mg of *N*-hydroxysuccinimide (NHS; Sigma-Aldrich), 249 mg of *N*-(3-dimethylaminopropyl)-*N*′-ethylcarbodiimide (EDC; Sigma-Aldrich), and 200 mg of DBCO-amine (Sigma-Aldrich). HA, EDC, and NHS were dissolved in 30 ml of 50 mM MES buffer (pH 4.0). DBCO-amine was dissolved in 3 ml of dimethyl sulfoxide (DMSO) before addition to HA-NHS-EDC solution. The reaction was carried out for 48 hours at room temperature. The reaction mixture was spin-concentrated using 10-kDa cutoff spin filters (Millipore), and HA-DBCO was precipitated with a fivefold excess of ice-cold acetone. Precipitate was pelleted at 4000*g* for 10 min and washed twice with ice-cold acetone. HA-DBCO was then dissolved in ultrapure water and frozen overnight at −80°C before lyophilizing to obtain solid HA-DBCO. Lyophilization was carried with a FreeZone 4.5L Freeze Drier (Labconco) using standard vacuum flasks at 0.133 bar and −40°C collector temperature for 72 hours.

Making hydrogels with tunable stress relaxation

Lyophilized HA-DBCO was first dissolved in DMEM/F-12 to make a stock solution of 10% (w/v) HA-DBCO. Azide-functionalized DNA side arms (az-SA, IDT) and linker constructs (Elimbio) were obtained commercially. az-SA1, az-SA2, and linker constructs were mixed separately and stored at 37°C in equimolar amounts with a final concentration of 150 μM. The DNA solution was then mixed with the 10% HA solution, cell suspension, RGD solution, and additional DMEM/F-12 to obtain a final mixture with 3.3% (w/v) HA-DBCO and RGD (0.5 mg/ml). PEG-az (Sigma-Aldrich) was dissolved at 5% (w/v) in ultrapure water, and 0.345 μl of PEG-az solution per 10 μl of 3.3% HA solution was added to initiate gelation.

Hydrogel characterization

Hydrogels were characterized via shear rheometry on an MCR 301 rheometer (Anton-Paar) using parallel plate geometry (20 mm diameter). All measurements were carried out in a prehumidified chamber at 37°C to prevent hydrogel drying. Gel samples were polymerized with a 200-μm thickness for 20 min on a rheometer heated stage. For stress relaxation measurements, a constant 15% strain was applied for 15 min. For initial elastic modulus measurements, oscillatory strain was applied with an amplitude of 0.5% and a frequency of 1 Hz.

Immunocytochemistry

We fixed the hydrogel samples by incubating them with 4% paraformaldehyde in phosphate-buffered saline (PBS) for 15 min at room temperature. Then, the samples were washed with PBS three times and permeabilized and blocked with Triton X-100 (0.3%) and bovine serum albumin (3%) in PBS for 35 min at room temperature. The samples were then incubated at 4°C for 48 hours with the following primary antibodies: mouse anti–tubulin β3 (TUBB3) (1:1000, BioLegend), rabbit anti-GFAP (1:1000, Abcam), mouse anti–β spectrin II (1:500, BD Biosciences), and rabbit anti–early growth response 1 (Egr1) (1:1000, Cell Signaling Technology). After washing with PBS for three times, the samples were incubated with goat anti-rabbit immunoglobulin G (IgG) (H+L) secondary antibody or Alexa Fluor 546 (Invitrogen) and goat anti-mouse IgG (H+L) secondary antibody, Alexa Fluor 633 conjugate (Invitrogen) for 24 hours at room temperature. 4′,6-Diamidino-2-phenylindole (DAPI; Sigma-Aldrich) and Alexa Fluor 546 Phalloidin (Thermo Fisher Scientific) were treated to label nuclei and F-actin, respectively. Fluorescence images were taken using Zeiss LSM 880 confocal laser scanning microscope, 60× and 40× objective lenses, and Zeiss ZEN microscopy software and visualized by z-stack mode. All image analysis and processing was performed with ImageJ, Imaris, Huygens, and Zeiss BLACK software. Structured illumination super-resolution imaging was performed on a Zeiss Elyra PS.1 epifluorescence microscope using a 100× objective lens. Additional fluorescence confocal imaging for 3D whole-gel imaging was performed on PerkinElmer Opera Phenix High-Content Screening System using a 40× objective lens.

Sectioning samples

The samples of cells encapsulated with hydrogels were fixed and embedded in OCT compound solution (Tissue-Tek) at −80°C for 30 min and sectioned to the thickness of 15 to 30 μm via a cryostat NX50 (Thermo Fisher Scientific). Sectioned samples were attached to Tissue Path Superfrost Plus Gold Slides (Fisher Scientific) and washed with PBS for three times. Then, the resulting samples were immunostained and used to characterize colocalization of F-actin and β spectrin II.

RNA isolation and qPCR

To extract only the cells, the hydrogels were lysed by incubating the samples in DMEM/F-12 containing hyaluronidase (750 to 3000 U/ml, Sigma-Aldrich) for 30 min at 37°C. The cells were then sorted down by centrifuging at 200*g* for 2 min to remove all the residuals and washed with PBS once. Phenol-free total RNA was extracted from the cell pellets using RNeasy Plus Micro Kit with gDNA eliminator columns (Qiagen) following the manufacturer's protocol. Total RNA concentration was measured by NanoDrop, and 600 ng of RNA was converted to cDNA using an iScript cDNA synthesis kit (Bio-Rad). The resulting cDNA was used for SYBR Green (Bimake) qPCR with a 5 μM final forward and reverse primer concentration. The mRNA expression levels of Sptbn1 and Egr1 were measured by using the following primers: *Sptbn1* (forward: 5′-ATGAGAGAGACATGGCTGAG-3′, reverse: 5′-TAGCTCTCTGCTTCAAGCTC-3′), *Egr1* (forward: 5′-GTATGCTTGCCCTGTTGAGTCC-3′, reverse: 5′-CATGCAGATTCGACACTGGAAG-3′), *18s* (forward: 5′-GTAACCCGTTGAACCCCATTC-3′, reverse: 5′-CCATCCAATCGGTAGTAGCGA-3′).

Western blotting

Hyaluronidase (750 to 3000 U/ml, Sigma-Aldrich) was treated to the samples at 37°C for 30 min to isolate only the NSCs. Then, resulting samples were centrifuged at 200*g* for 2 min to remove all the residuals (suspension). The cell pellet was resuspended with PBS once and lysed with radioimmunoprecipitation assay (RIPA) lysis buffer (Sigma-Aldrich) containing Halt proteinase and phosphatase inhibitor cocktail (Thermo Fisher Scientific) on ice for 10 min to extract total protein. The protein concentration was measured by bicinchoninic acid (BCA) assay with Pierce BCA protein assay kit (Thermo Fisher Scientific), and samples were normalized with respect to the total protein content. Proteins were separated via SDS–polyacrylamide gel electrophoresis (PAGE) and transferred onto a nitrocellulose membranes (0.22 μm, Odyssey). A tris-buffered saline (TBS) blocking buffer (Odyssey) was treated to the membrane

to block for 40 min, and the resulting membrane was incubated overnight at 4°C with following primary antibodies: mouse anti–β spectrin II (1:500, BD Biosciences), rabbit anti-Egr1 (1:1000, Cell Signaling Technology), and mouse anti–β-actin (1:10,000, Sigma-Aldrich). The membranes were then washed with Tris-buffered saline with 0.1% Tween 20 (TBST) and treated with biotinylated secondary antibodies [goat anti-rabbit IgG H&L (biotin) (1:10,000, Abcam) or goat anti-mouse IgG H&L (biotin) (1:10,000, Abcam)]. After washing with TBST for three times, streptavidin-conjugated fluorescent label [Streptavidin, Alexa Fluor 790 conjugate (Invitrogen) or Streptavidin, Alexa Fluor 700 conjugate (Invitrogen)] was treated with the concentration of 1:10,000 to the membranes. The membranes were then washed with TBST again and imaged by Odyssey CLx (LI-COR Biosciences).

shRNA cloning

shRNA inserts were designed using Ensembl genome browser and the online tool (InvivoGen) as follows: shSptbn1-1, GAGCATGTCACGATGTTACAA; shSptbn1-2, GAAGAAATCGAATGCACACTA; shSptbn1-3, TGGATGAAATGAAGGTGCTAT; shCtrl, ACCTAAGAGCAGCAAATAAT. The inserts were obtained from Elim Biopharmaceuticals and ligated into the pLKO.1 puro vector (Addgene plasmid #10878).

Viral packaging and transduction

The cloned plasmid, psPAX2, and pMD2.G were used to package lentiviral particles through polyethylenimine (PEI) transfection of human embryonic kidney (HEK) 293T cells and purified as previously described (*42*). Then, the purified viral particles were transduced to the NSCs with multiplicity of infection (MOI) of 1. The puromycin-resistant shRNA-expressing cells were selected using puromycin (1 μg/ml) longer than 4 days.

Image analysis

Immunofluorescence images of the cells encapsulated within 3D gels for 5 hours after gel dissection were used for the intensity quantification of F-actin, β spectrin II, and EGR1. The intensity was determined by using Fiji. Fluorescent images showing 3D rendering of single NSCs stained with cell membrane dye (R18) were used to quantify the cell volume. The volume was measured by using Imaris 3D imaging software. SIM analysis was performed in Zeiss BLACK software using the built-in SIM processing tool. SIM-processed images were then channel-aligned using calibration data from fluorescent beads. Further postprocessing was performed using Huygens analysis software (Scientific Volume Imaging) for image deconvolution. Manders colocalization coefficients were calculated in Huygens using the Costes background estimation.

Abaqus simulation

The effect of the stress relaxation of hydrogels on the confining stress of the cell was analyzed using a commercial finite element method tool (ABAQUS v 6.24). A spherical cell and the hexahedron-shaped hydrogel were modeled as a 3D, deformable solid with 207,194 nodes and 140,779 elements of type C3D10 (10-node quadratic tetrahedron). The radius of the cell was determined from experimentally measured volumes, and the length of each side of the hydrogel was assumed to be 100 μm. The cell was located at the center of the hydrogel, and a symmetric boundary condition was applied to reduce computational costs. The cell was considered to be purely elastic with a constant modulus of 500 Pa and Poisson's ratio of 0.49, while the hydrogel was considered to be viscoelastic material with experimentally obtained relaxation modulus fitted by Prony series and Poisson's ratio of 0.49.

Statistical analysis

All the quantitative data were presented as the mean ± SD, and the number of biological and technical replicates is indicated in the figure legends and Materials and Methods. One-way analysis of variance (ANOVA) followed by Tukey test and Student's *t* test for between-group differences was performed with GraphPad Prism as indicated in the figure legends.

Note added in proof: After acceptance, the authors became aware of a recently published paper (*43*).This added reference was not published at the time of the paper's acceptance.

Supplementary Materials

This PDF file includes:
Figs. S1 to S5
Legends for movies S1 and S2

Other Supplementary Material for this manuscript includes the following:
Movies S1 and S2

REFERENCES AND NOTES

1. C. R. Keese, I. Giaever, Substrate mechanics and cell spreading. *Exp. Cell Res.* **195**, 528–532 (1991).
2. A. J. Engler, L. Richert, J. Y. Wong, C. Picart, D. E. Discher, Surface probe measurements of the elasticity of sectioned tissue, thin gels and polyelectrolyte multilayer films: Correlations between substrate stiffness and cell adhesion. *Surf. Sci.* **570**, 142–154 (2004).
3. K. A. Beningo, C.-M. Lo, Y.-L. Wang, Flexible polyacrylamide substrata for the analysis of mechanical interactions at cell-substratum adhesions. *Methods Cell Biol.* **69**, 325–339 (2002).
4. A. Jannatbabaei, M. Tafazzoli-Shadpour, E. Seyedjafari, N. Fatouraee, Cytoskeletal remodeling induced by substrate rigidity regulates rheological behaviors in endothelial cells. *J. Biomed. Mater. Res. A* **107**, 71–80 (2019).
5. S. Vichare, S. Sen, M. M. Inamdar, Cellular mechanoadaptation to substrate mechanical properties: Contributions of substrate stiffness and thickness to cell stiffness measurements using AFM. *Soft Matter* **10**, 1174–1181 (2014).
6. Q. Wang, J. Xie, C. Zhou, W. Lai, Substrate stiffness regulates the differentiation profile and functions of osteoclasts via cytoskeletal arrangement. *Cell Prolif.* **55**, e13172 (2022).
7. P. C. Georges, W. J. Miller, D. F. Meaney, E. S. Sawyer, P. A. Janmey, Matrices with compliance comparable to that of brain tissue select neuronal over glial growth in mixed cortical cultures. *Biophys. J.* **90**, 3012–3018 (2006).
8. A. Engler, L. Bacakova, C. Newman, A. Hategan, M. Griffin, D. Discher, Substrate compliance versus ligand density in cell on gel responses. *Biophys. J.* **86**, 617–628 (2004).
9. E. M. Carvalho, S. Kumar, Lose the stress: Viscoelastic materials for cell engineering. *Acta Biomater.* **163**, 146–157 (2023).
10. J. Lou, R. Stowers, S. Nam, Y. Xia, O. Chaudhuri, Stress relaxing hyaluronic acid-collagen hydrogels promote cell spreading, fiber remodeling, and focal adhesion formation in 3D cell culture. *Biomaterials* **154**, 213–222 (2018).
11. Z. Gong, S. E. Szczesny, S. R. Caliari, E. E. Charrier, O. Chaudhuri, X. Cao, Y. Lin, R. L. Mauck, P. A. Janmey, J. A. Burdick, V. B. Shenoy, Matching material and cellular timescales maximizes cell spreading on viscoelastic substrates. *Proc. Natl. Acad. Sci. U.S.A.* **115**, E2686–E2695 (2018).
12. O. Chaudhuri, J. Cooper-White, P. A. Janmey, D. J. Mooney, V. B. Shenoy, Effects of extracellular matrix viscoelasticity on cellular behaviour. *Nature* **584**, 535–546 (2020).
13. M. Kamkar, M. Janmaleki, E. Erfanian, A. Sanati-Nezhad, U. Sundararaj, Viscoelastic behavior of covalently crosslinked hydrogels under large shear deformations: An approach to eliminate wall slip. *Phys. Fluids* **33**, 41702 (2021).
14. F. Charbonier, D. Indana, O. Chaudhuri, Tuning viscoelasticity in alginate hydrogels for 3D cell culture studies. *Curr. Protoc.* **1**, e124 (2021).
15. B. M. Richardson, C. J. Walker, L. J. Macdougall, J. W. Hoye, M. A. Randolph, S. J. Bryant, K. S. Anseth, Viscoelasticity of hydrazone crosslinked poly(ethylene glycol) hydrogels directs chondrocyte morphology during mechanical deformation. *Biomater. Sci.* **8**, 3804–3811 (2020).

16. M. Reimer, S. Petrova Zustiak, S. Sheth, J. Martin Schober, Intrinsic response towards physiologic stiffness is cell-type dependent. *Cell Biochem. Biophys.* **76**, 197–208 (2018).
17. D. Choquet, D. P. Felsenfeld, M. P. Sheetz, Extracellular matrix rigidity causes strengthening of integrin-cytoskeleton linkages. *Cell* **88**, 39–48 (1997).
18. S. V. Plotnikov, A. M. Pasapera, B. Sabass, C. M. Waterman, Force fluctuations within focal adhesions mediate ECM-rigidity sensing to guide directed cell migration. *Cell* **151**, 1513–1527 (2012).
19. J. Baek, P. A. Lopez, S. Lee, T.-S. Kim, S. Kumar, D. V. Schaffer, *Egr1* is a 3D matrix-specific mediator of mechanosensitive stem cell lineage commitment. *Sci. Adv.* **8**, eabm4646 (2022).
20. A. J. Keung, E. M. de Juan-Pardo, D. V. Schaffer, S. Kumar, Rho GTPases mediate the mechanosensitive lineage commitment of neural stem cells. *Stem Cells* **29**, 1886–1897 (2011).
21. K. L. Perkins, A. M. Arranz, Y. Yamaguchi, S. Hrabetova, Brain extracellular space, hyaluronan, and the prevention of epileptic seizures. *Rev. Neurosci.* **28**, 869–892 (2017).
22. B. S. Spearman, N. K. Agrawal, A. Rubiano, C. S. Simmons, S. Mobini, C. E. Schmidt, Tunable methacrylated hyaluronic acid-based hydrogels as scaffolds for soft tissue engineering applications. *J. Biomed. Mater. Res. A* **108**, 279–291 (2020).
23. S.-S. Han, H. Y. Yoon, J. Y. Yhee, M. O. Cho, H.-E. Shim, J.-E. Jeong, D.-E. Lee, K. Kim, H. Guim, J. H. Lee, K. M. Huh, S.-W. Kang, In situ cross-linkable hyaluronic acid hydrogels using copper free click chemistry for cartilage tissue engineering. *Polym. Chem.* **9**, 20–27 (2018).
24. T. Ito, I. P. Fraser, Y. Yeo, C. B. Highley, E. Bellas, D. S. Kohane, Anti-inflammatory function of an in situ cross-linkable conjugate hydrogel of hyaluronic acid and dexamethasone. *Biomaterials* **28**, 1778–1786 (2007).
25. S. Rammensee, M. S. Kang, K. Georgiou, S. Kumar, D. V. Schaffer, Dynamics of mechanosensitive neural stem cell differentiation. *Stem Cells* **35**, 497–506 (2017).
26. A. G. Clark, O. Wartlick, G. Salbreux, E. K. Paluch, Stresses at the cell surface during animal cell morphogenesis. *Curr. Biol.* **24**, R484–R494 (2014).
27. G. Salbreux, G. Charras, E. Paluch, Actin cortex mechanics and cellular morphogenesis. *Trends Cell Biol.* **22**, 536–545 (2012).
28. R. K. H. Liem, Cytoskeletal integrators: The spectrin superfamily. *Cold Spring Harb. Perspect. Biol.* **8**, a018259 (2016).
29. R. Zhang, C. Zhang, Q. Zhao, D. Li, Spectrin: Structure, function and disease. *Sci. China Life Sci.* **56**, 1076–1085 (2013).
30. N. Unsain, F. D. Stefani, A. Cáceres, The actin/spectrin membrane-associated periodic skeleton in neurons. *Front. Synaptic Neurosci.* **10**, 10 (2018).
31. M. W. Nestor, X. Cai, M. R. Stone, R. J. Bloch, S. M. Thompson, The actin binding domain of βI-spectrin regulates the morphological and functional dynamics of dendritic spines. *PLOS ONE* **6**, e16197 (2011).
32. P. H. Kang, D. V. Schaffer, S. Kumar, Angiomotin links ROCK and YAP signaling in mechanosensitive differentiation of neural stem cells. *Mol. Biol. Cell* **31**, 386–396 (2020).
33. D. Indana, P. Agarwal, N. Bhutani, O. Chaudhuri, Viscoelasticity and adhesion signaling in biomaterials control human pluripotent stem cell morphogenesis in 3D culture. *Adv. Mater.* **33**, e2101966 (2021).
34. O. Chaudhuri, L. Gu, D. Klumpers, M. Darnell, S. A. Bencherif, J. C. Weaver, N. Huebsch, H.-P. Lee, E. Lippens, G. N. Duda, D. J. Mooney, Hydrogels with tunable stress relaxation regulate stem cell fate and activity. *Nat. Mater.* **15**, 326–334 (2016).
35. Y.-P. Lo, Y.-S. Liu, M. G. Rimando, J. H.-C. Ho, K.-H. Lin, O. K. Lee, Three-dimensional spherical spatial boundary conditions differentially regulate osteogenic differentiation of mesenchymal stromal cells. *Sci. Rep.* **6**, 21253 (2016).
36. M. Caiazzo, Y. Okawa, A. Ranga, A. Piersigilli, Y. Tabata, M. P. Lutolf, Defined three-dimensional microenvironments boost induction of pluripotency. *Nat. Mater.* **15**, 344–352 (2016).
37. M. Bao, J. Xie, A. Piruska, W. T. S. Huck, 3D microniches reveal the importance of cell size and shape. *Nat. Commun.* **8**, 1962 (2017).
38. X.-T. Wu, L.-W. Sun, X. Yang, D. Ding, D. Han, Y.-B. Fan, The potential role of spectrin network in the mechanotransduction of MLO-Y4 osteocytes. *Sci. Rep.* **7**, 40940 (2017).
39. R. G. Sampayo, M. Sakamoto, M. Wang, S. Kumar, D. V. Schaffer, Mechanosensitive stem cell fate choice is instructed by dynamic fluctuations in activation of Rho GTPases. *Proc. Natl. Acad. Sci. U.S.A.* **120**, e2219854120 (2023).
40. T. D. Palmer, E. A. Markakis, A. R. Willhoite, F. Safar, F. H. Gage, Fibroblast growth factor-2 activates a latent neurogenic program in neural stem cells from diverse regions of the adult CNS. *J. Neurosci.* **19**, 8487–8497 (1999).
41. S. Y. Wang, H. Kim, G. Kwak, H. Y. Yoon, S. D. Jo, J. E. Lee, D. Cho, I. C. Kwon, S. H. Kim, Development of biocompatible HA hydrogels embedded with a new synthetic peptide promoting cellular migration for advanced wound care management. *Adv. Sci.* **5**, 1800852 (2018).
42. J. Peltier, D. V. Schaffer, Viral packaging and transduction of adult hippocampal neural progenitors. *Methods Mol. Biol.* **621**, 103–116 (2010).
43. E. Qiao, C. A. Fulmore, D. V. Schaffer, S. Kumar, Substrate stress relaxation regulates neural stem cell fate commitment. *Proc. Natl. Acad. Sci. U.S.A.* **121**, e2317711121(2024).

Acknowledgments: We thank M. West (California Institute for Quantitative Biosciences High-Throughput Screening Facility) and D. Schichnes (Berkeley Biological Imaging Facility) for imaging and microscopy assistance. A figure was created with BioRender.com. **Funding:** This work was supported by NIH grant R01NS074831 (S.K. and D.V.S.) and NIH training program T32GM098218 (E.Q.). **Author contributions:** Conceptualization: S.K., D.V.S., E.Q., and J.B. Methodology: E.Q. and J.B. Investigation: E.Q., J.B., C.F., M.S., and T.-S.K. Visualization: E.Q. and J.B. Supervision: S.K. and D.V.S. Writing—original draft: E.Q. and J.B. Writing—review and editing: S.K., D.V.S., C.F., M.S., and T.-S.K. Resources: E.Q., J.B., S.K., and D.V.S. Data curation: E.Q., J.B., and C.F. Validation: E.Q. and J.B. Formal analysis: E.Q., C.F., and T.-S.K. Software: E.Q. and C.F. Project administration: E.Q., J.B., S.K., and D.V.S. Funding acquisition: D.V.S. and S.K. **Competing interests:** The authors declare that they have no competing interests. **Data and materials availability:** All data needed to evaluate the conclusions in the paper are present in the paper and/or the Supplementary Materials. Materials can be provided by the corresponding authors pending scientific review and a completed material transfer agreement. Requests for the specific materials should be submitted to the corresponding authors.

Submitted 24 September 2023
Accepted 27 June 2024
Published 2 August 2024
10.1126/sciadv.adk8232